Colloids and Surfaces B: Biointerfaces 110 (2013) 485–488

Contents lists available at SciVerse ScienceDirect

Colloids and Surfaces B: Biointerfaces

journal homepage: www.elsevier.com/locate/colsurfb

Short communication

DNA functionalized gold nanorods/nanoplates assembly as sensitive LSPR-based sensor for label-free detection of mercury ions

Dandan Li[a,b], Guangchao Zheng[a,b], Xiaofeng Ding[a], Jin Wang[a,b,*], Jinhuai Liu[a], Lingtao Kong[a]

[a] Research Center for Biomimetic Functional Materials and Sensing Devices, Institute of Intelligent Machines, Chinese Academy of Sciences, Hefei, Anhui 230031, China
[b] College of Chemistry and Material Science, University of Science and Technology of China, Anhui 230026, China

ARTICLE INFO

Article history:
Received 22 January 2013
Received in revised form 24 March 2013
Accepted 17 April 2013
Available online 30 April 2013

Keywords:
DNA
Assembly
LSPR
Label-free
Mercury

ABSTRACT

Core–satellite assembly, *i.e.*, gold nanoplates (AuNPs) surrounded by gold nanorods (AuNRs), has been obtained by Thymine–Hg^{2+}–Thymine (T–Hg^{2+}–T) coordination. A novel label-free localized surface plasmon resonance (LSPR) detection of mercury ions can be performed *via* the core–satellite assembly. The proposed detection protocol exhibits good linear correlation between wavelength shifts of the plasmon band and concentrations of mercury ions over the range from 10 nM to 0.2 μM. Moreover, the detection limit (3σ) for the probes is 2.2 nM, which is better than colorimetric detection *via* random aggregation of gold nanoparticles.

1. Introduction

Detecting mercury contaminations in ecosystem is an important issue around the world due to their toxic nature and non-biodegradable properties, which lead to various damages to the central nervous system, immune system and endocrine system. The World Health Organization (WHO) standard for the maximum allowable level of inorganic mercury in drinking water is lower than 6 ppb [1,2]. Recently, many optoelectric methods, *e.g.*, fluorescence [3–5], surface enhanced Raman scattering (SERS) [6–9], electrochemistry [10,11], have been widely utilized for monitoring mercury ions. In contrast, low-cost colorimetric approaches based on aggregations of gold nanoparticles (AuNPs) *via* Thymine–Hg^{2+}–Thymine coordination are being employed for detecting mercury ions [12–14]. However, sensitivity of colorimetric approach is low compared to some other optical methods, *e.g.*, SERS or fluorescence *etc*. Herein, we propose a sensitive *in situ* probing protocol for determining mercury levels, *i.e.*, mercury (II) mediated assembly between Thymine-rich ss-DNA functionalized gold nanorods (AuNRs) and nanoplates (AuNPs), which is different from random aggregation of AuNPs.

2. Materials and methods

2.1. Materials

$HAuCl_4{\cdot}4H_2O$ (99.9%), $NaBH_4$ (99%), vitamin C (99.9%), CTAB (99%) and $AgNO_3$ (99.9%), KI (99.9%), tri-sodium citrate (99.9%), 3-N-morpholinopropanesulfonic acid (MOPS), phosphate buffer (PBS) were purchased from Aldrich. Mercury nitrate and other metal salts were purchased from Beijing Chem. Reagent Ltd. (Beijing, China). DNA oligomers were purchased from Sangon (Shanghai, China) and used without further purification. All experiments were carried out in aqueous MOPs buffer (10 mM MOPs with 50 mM $NaNO_3$, pH 7.2) solution. The double distilled (DI) water that was used throughout the experiments was purified by using a Milli-Q system.

2.2. Preparation of gold nanorods and nanoplates

2.2.1. Gold nanorods (AuNRs)

AuNRs were synthesized through seed-mediated approach, which has been described in our previous report [15]. The preparation of gold seed solution and growth solution can be carried out independently. 600 μL 0.02 M ice-cold $NaBH_4$ was added to

* Corresponding author at: Research Center for Biomimetic Functional Materials and Sensing Devices, Institute of Intelligent Machines, Chinese Academy of Sciences, Hefei, Anhui 230031, China. Tel.: +86 65595607; fax: +86 65592420.
E-mail address: jwang@iim.ac.cn (J. Wang).

0927-7765/$ – see front matter © 2013 Elsevier B.V. All rights reserved.
http://dx.doi.org/10.1016/j.colsurfb.2013.04.039

the vigorously stirred solution including 10 mL 0.5 mM $HAuCl_4$ and 10 mL 0.2 M CTAB mixtures for 2 min, which resulted in the formation of brown-yellow gold seeds. Subsequently, the gold seed solution had been kept at 25 °C for 2 h before it was used for preparing AuNRs. As for the gold growth solution, it was prepared from 100 mL 0.2 M CTAB, 10 mL 4 mM $AgNO_3$, 100 mL 1 mM $HAuCl_4$ solution and 1.4 mL 0.08 M vitamin C at room temperature. Finally, 0.24 mL seed solution was added to the as-prepared growth solution to form AuNRs, and settled at 27 °C for overnight. The AuNRs were centrifuged at 10,000 rpm for 10 min and redispersed in 20 mL DI water.

2.2.2. Gold nanoplates (AuNPs)

Three-step seed-mediated synthesis of AuNPs could be referred to our previous report [16]. 0.5 mL 10 mM sodium citrate and 0.5 mL 10 mM $HAuCl_4$ were diluted to 20 mL aqueous solution. 0.5 mL 100 mM $NaBH_4$ was quickly added to the mixtures and stirred for 2 min so as to generate gold seeds. Then, the gold seeds have been kept for 2 h at room temperature. As for gold growth solution, the mixture including 0.625 mL 0.01 M $HAuCl_4$, 22.5 mL 0.05 M CTAB, 0.125 mL 0.1 M NaOH, 0.125 mL 0.1 M vitamin C, 0.1 mL 0.01 M KI, was stored in vial A. Subsequently, 2.25 mL gold growth solution was transferred from the vial A to vial B, and 250 μL solution was transferred from the vial B to vial C. The AuNPs were yielded through the following three-step process. Firstly, 22.5 μL gold seed solution was added to the vial C and stirred for 3 s. Then, all of the solution in the vial C was immediately added to the *via* B and stirred for 3 s. Finally, all of the solution in the vial B was transferred to the vial A for settled for overnight. The as-prepared AuNPs were centrifuged at 6000 rpm for 10 min and redispersed in 20 mL DI water.

2.3. LSPR sensing of mercury ions

DNA oligomers with a sequence of SH-5′-CTTGTCAGCT-TGGCTTTGT-3′ were added to the AUNRs at a ratio of 800:1 in 0.01 M phosphate buffer (PBS: 137 mM NaCl, 2.5 mM Mg^{2+}, 10 mM Na_2HPO_4, and 2.0 mM KH_2PO_4, pH 7.4) and incubated at 25 °C in a shaker for overnight. In order to obtain core–satellite nanogold assembly, the ss-DNA with a sequence of SH-5′-ACTTTGCCTTGCTGACTTG-3′ was added to the AuNPs with a ratio of DNA to the AuNPs under *ca.* 100:1. The conjugated process could be allowed to react at 25 °C in a shaker for overnight. The ss-DNA-AuNRs and ss-DNA-AuNPs conjugates were collected after centrifugation for 10 min at 10,000 rpm and 6000 rpm, respectively, and dispersed in DI water and stored at 4 °C. The mixture including ss-DNA-AuNRs and ss-DNA-AuNPs was incubated with Hg^{2+} of a series of concentrations 1×10^{-8} M, 2×10^{-8} M, 6×10^{-8} M, 9×10^{-8} M, 1.5×10^{-7} M, 2×10^{-7} M in a MOPS (3-N-morpholinopropaneousulfonic acid) buffer (10 mM with 50 mM $NaNO_3$, PH 7.2) for 0.5 h. UV–vis-NIR spectra were recorded for LSPR sensing of mercury ions.

2.4. Characterization

Transmission electron microscopy (TEM) images were acquired with a JEM-2011 operating at 200 kV. Scanning electron microscopy (SEM) was acquired with a Quanta200FEG. The ultraviolet–visible–near infrared (UV–vis–NIR) spectra were recorded in quartz cuvettes with a SOLID 3700 spectrophotometer. DLS experiments can be performed *via* Beckman Coulter Relsa Nanoparticle analyzer.

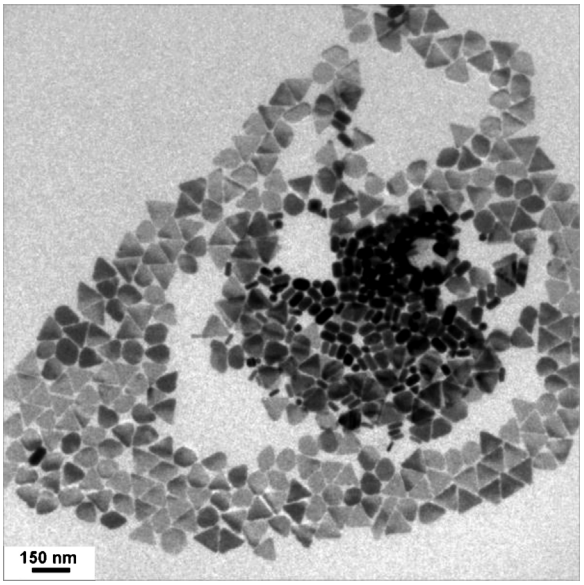

Fig. 1. Mixture of ss-DNA-AuNRs and ss-DNA-AuNPs without assembly.

3. Results and discussion

Fig. S1 shows that monodispersed AuNRs with aspect ratio *ca.* 2.5–3 could be obtained *via* seed-mediated approach. Two plasmon modes of the AuNRs, *i.e.*, transverse and longitudinal modes located at 525 nm and 635 nm, respectively, could be observed in Fig. S2a. AuNPs with edge length *ca.* 90–110 nm can be yielded through the three-step seed-mediated method (shown in Fig. S3). Their high purities could be reflected from strong dipole SPR excitation at 1090 nm and disappearance of SPR excitation at 520 nm in UV–vis–NIR spectrum (see Fig. S4a). Hence, pure AuNPs and AuNRs have been chosen as assembled substrates. Furthermore, obvious broadening or shift of localized SPRs of the AuNRs and the AuNPs could not be observed after DNA conjugation (refer to Figs. S2b and S4b), indicating that ss-DNA functionalization did not cause aggregations of the AuNRs and the AuNPs.

As far as assembled superstructures are concerned, core–satellite plasmonic structures are quite interesting because of their unique LSPR properties, which lead to promising applications in surface enhanced Raman scattering [17], LSPR sensor [18], plasmon rulers [19] *etc.* In the present case, the core–satellite assembly, *i.e.*, the AuNPs at the centre serving as core and the AuNRs encircling the core as satellite, can be described in Fig. S5. In the case of the AuNPs, crystal facets exhibit different surface energies and chemical reactivities, *e.g.*, low reactivity of {1 1 1} face in contrast to {1 1 0} or {1 0 0} [20]. Thereby, edges of the AuNPs tend to more easily react with thiolated ss-DNA in contrast to triangular faces. In order to yield core–satellite plasmonic structure, the ss-DNA conjugated with the AuNPs should be controlled with the ratio of DNA to the AuNPs under 100. Thymine-rich DNA functionalized AuNRs and AuNPs are difficult to be assembled without addition of mercury ions due to T–T mismatch. As observed from TEM in Fig. 1, depletion attraction between the AuNRs and the AuNPs can cause phase separation, *e.g.*, exclusive rods-rich and plate-rich region. Accompany with addition of mercury ions, ss-DNA functionalized AuNRs/AuNPs assembly can be formed *via* T–Hg^{2+}–T coordination. It can be assumed that there are three types of assembled pattern, *i.e.*, parallel, vertical and quasi-parallel pattern in AuNRs/AuNPs assembly (shown in Fig. S6). Fig. 2 and Fig. S7 TEM results indicate that more AuNRs tend to be assembled around AuNPs in parallel pattern, that is, percentage of parallel assembly is relatively higher in contrast to vertical assembly. It should be pointed out that

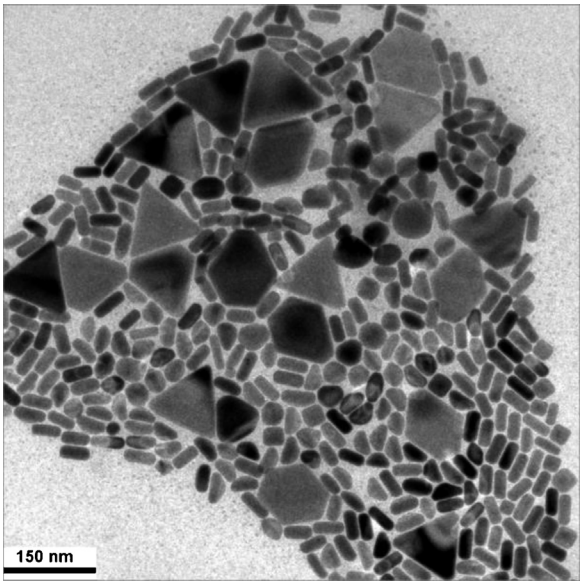

Fig. 2. TEM morphology of AuNRs/AuNPs assembly.

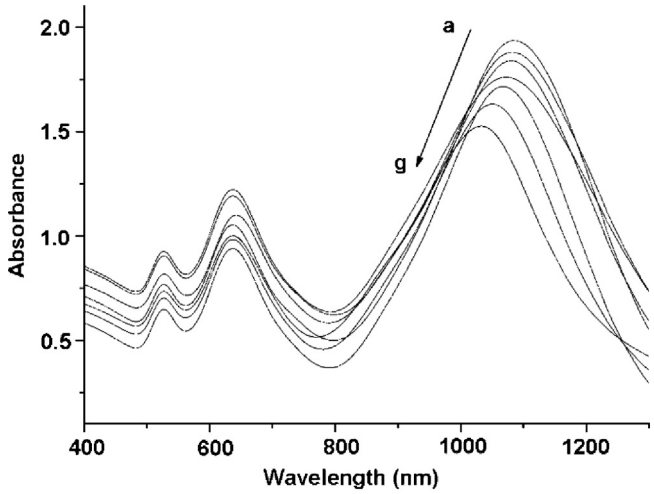

Fig. 3. UV–vis–NIR absorbance spectra of ss-DNA functionalized AuNRs/AuNPs assembly (a) without mercury ions, (b–g) after the addition of mercury ions at different concentrations (0.01, 0.02, 0.06, 0.09, 0.15, 0.2 μM).

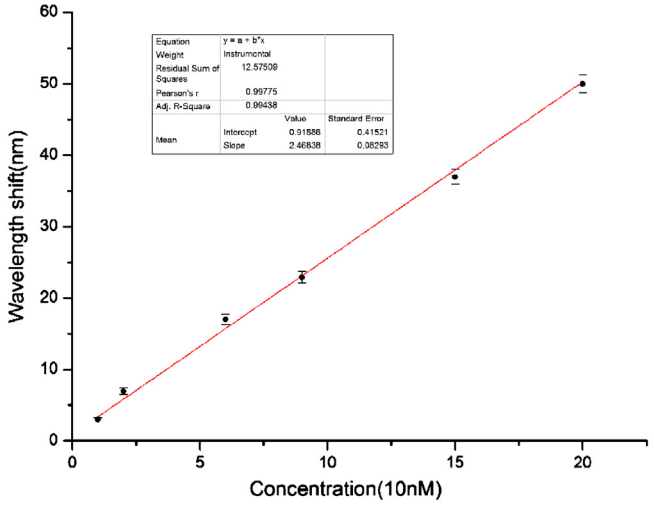

Fig. 4. The relationship between wavelength shift and mercury ions concentrations ranged from 10 nM to 200 nM. Each of points is the average of five detection data and shown with a standard error bar.

the formation of core–satellite assembly needs to be carefully controlled by optimized experimental condition. For example, as shown in Fig. S8, AuNPs with etched edge are unfavorable for assembling the AuNRs around edge of the AuNPs. Additionally, excess amounts of DNA conjugated on the AuNPs can easily lead to the AuNRs absorbed on the triangular {1 1 1} plane, which inhibit their assemblies along the edge of AuNPs (see Fig. S9). The AuNRs/AuNPs assembly should be characterized *via* dynamic light scattering (DLS) in order to exclude the arrangement from capillary forces between nanoparticles and substrates during solvent vaporation in the TEM sample preparation. The average hydrodynamic diameters (AHD) of the AuNRs and the AuNPs are *ca.* 45 nm and 96 nm in Fig. S10 and S11, respectively, which are consistent with TEM observations. As far as AHD of the AuNRs/AuNPs assembly *via* 10 nM and 200 nM mercury ions are concerned, sizes of the assembly could be measured as 145.2 nm (Fig. S12) and 216.3 nm (Fig. S13), respectively. Hence, obvious increase of AHD for the AuNRs/AuNPs assembly could be observed, suggesting that self-assembly should be formed in solution.

As far as absorption pattern of the AuNRs are concerned, vertical assembly can cause dipole plasmon mode of the AuNPs parallel to axis of the AuNRs, which lead to red-shift of dipole plasmon mode. On the contrary, parallel assembly can cause dipole plasmon mode of the AuNPs vertical to axis of the AuNRs, which is responsible to blue-shift of dipole plasmon mode. As observed from TEM experiments, dominant parallel assembly between the AuNRs and the AuNPs directly leads to continuous blue-shift of strong dipole plasmon bands of the AuNPs in NIR region accompany with addition of amounts of mercury ions (shown in Fig. 3). The wavelength shift of dipole plasmon bands of the AuNPs in the core–satellite assembly has a good linear correlation (correlation constant *ca.* 0.9977) (shown in Fig. 4 inset graph) with the concentrations of mercury ions from 10 nM to 0.2 μM. Each of the data points was the average of five detection data, and the relative deviations are calculated to be 7.91%, 6.63%, 4.12%, 3.48%, 2.85% and 2.55% for each of the six different concentration. The limit of detection was calculated to be 2.2 nM (0.44 ppb), based on S/N = 3. If amounts of mercury ions are relatively high, coordination between ss-DNA functionalized AuNPs and AuNRs leads to broadening of LSPR bands in the assembly, which cause deviation of maxima of LSPR bands. Hence, the present sensing protocol is appropriate for detection of mercury ions with low concentrations. It should be mentioned that shift for longitudinal plasmon bands of the AuNRs is very small, which is attributable to globally isotopic phase with local smectic structure in the assembly. The selectivity of the assembly has also been tested *via* LSPR shift response of some other ions, *e.g.*, Mg^{2+}, Cd^{2+}, Fe^{2+}, Cu^{2+}, Pb^{2+}, Ni^{2+}, Zn^{2+}, Na^{+}, at the concentration of 20 μM. In contrast with these heavy metal ions, as shown in Fig. S14, the remarkable LSPR shift of mercury ions-mediated assembly, suggesting that the present sensing protocol possesses excellent selectivity.

In conclusion, label-free LSPR sensor of mercury ions has been obtained *via* T–T mismatched AuNRs/AuNPs assembly and excellent sensitivity (LOD = 2.2 nM or 0.44 ppb) could be achieved compared to colorimetric sensor based on random aggregation of gold nanoparticles [21,22]. The facile LSPR sensor is superior to SERS or fluorescent sensor in that it does not need specific Raman or fluorescence labels.

Acknowledgements

This work is supported by the National Natural Science Foundation of China (Grant No. 21077106), National Key Scientific Program-Nanoscience and Nanotechnology (Grant No.

2011CB933700), Innovation fund for talented personnel of Anhui Province (2009Z035).

Appendix A. Supplementary data

Supplementary data associated with this article can be found, in the online version, at http://dx.doi.org/10.1016/j.colsurfb.2013.04.039.

References

[1] Y. Takahashi, S. Danwittayakul, T.M. Suzuki, Analyst 134 (2009) 1380.
[2] World Health Organization, Guideline for Drinking Water Quality, vol. 1, 2nd ed., World Health Organization, Geneva, Switzerland, 1993.
[3] M. Li, Q.Y. Wang, X.D. Shi, L.A. Hornak, N.Q. Wu, Anal. Chem. 83 (2011) 7061.
[4] C.I. Wang, C.C. Huang, Y.W. Lin, W.T. Chen, H.T. Chang, Anal. Chim. Acta 745 (2012) 124.
[5] B. Liu, Biosens. Bioelectron. 24 (2008) 756.
[6] D.H. Han, S.Y. Lim, B.J. Kim, L.L. Pian, T.D. Chung, Chem. Commun. 46 (2010) 5587.
[7] W. Ren, C. Zhu, E. Wang, Nanoscale 4 (2012) 5902.
[8] G.Q. Wang, C.S. Lim, L.X. Chen, H. Chon, J. Choo, J. Hong, A.J. DeMello, Anal. Biochem. 394 (2009) 1827.
[9] E. Chung, R. Gao, J. Ko, N. Choi, D.W. Lim, E.K. Lee, S. Chang, J. Choo, Lab Chip 13 (2013) 260.
[10] X. Tang, H. Liu, B. Zou, D. Tian, H. Huang, Analyst 137 (2012) 309.
[11] Z. Zhu, Y. Su, J. Li, D. Li, J. Zhang, S. Song, Y. Zhao, G. Li, C. Fan, Anal. Chem. 81 (2009) 7660.
[12] Z.H. Qing, X.X. He, K.M. Wang, Z. Zhou, X. Yang, J. Huang, G.P. Yan, Anal. Methods 4 (2012) 3320.
[13] F. Xia, X.L. Zuo, R.Q. Yang, Y. Xiao, D. Kang, A. Vallée-Bélisle, X. Gong, J.D. Yuen, B.B.Y. Hsu, A.J. Heeger, K.W. Plaxco, PNAS 107 (2010) 10837.
[14] X.J. Xue, F. Wang, X.G. Liu, J. Am. Chem. Soc. 130 (2008) 3244.
[15] J. Wang, L.T. Kong, Z. Guo, J.Y. Xu, J.H. Liu, J. Mater. Chem. 20 (2010) 5271.
[16] J.Y. Xu, J. Wang, L.T. Kong, G.C. Zheng, G. Zheng, J.H. Liu, J. Raman Spectrosc. 42 (2011) 1728.
[17] L.G. Xu, H. Kuang, C.L. Xu, W. Ma, L.B. Wang, N.A. Kotov, J. Am. Chem. Soc. 134 (2011) 1699.
[18] J.B. Lassiter, H. Sobhani, J.A. Fan, J. Kundu, F. Capasso, P. Nordlander, N.J. Halas, Nano Lett. 10 (2010) 3184.
[19] N. Liu, M. Hentschel, T. Weiss, A.P. Alivisatos, H. Giessen, Science 332 (2011) 1407.
[20] D. Aherne, D.M. Ledwith, M. Gara, J.M. Kelly, Adv. Funct. Mater. 18 (2008) 2005.
[21] Y.M. Guo, Z. Wang, W.S. Qu, H.W. Shao, X.Y. Jiang, Biosens. Bioelectron. 26 (2011) 4064.
[22] C.W. Liu, Y.T. Hsieh, C.C. Huang, Z.H. Lin, H.T. Chang, Chem. Commun. 19 (2008) 2242.